Probing the Photoreaction Mechanism of Phytochrome through Analysis of Resonance Raman Vibrational Spectra of Recombinant Analogues†

Frank Andel III,‡,§ John T. Murphy,||,⊥ Jeff A. Haas,||,# Michael T. McDowell,|| Ineke van der Hoef,▽ Johan Lugtenburg,▽ J. Clark Lagarias,|| and Richard A. Mathies*,‡

Department of Chemistry, University of California, Berkeley, California 94720, Section of Molecular and Cell Biology, University of California, Davis, California 95616, and Leiden Institute of Chemistry, University of Leiden, 2300 RA Leiden, The Netherlands

Received July 21, 1999; Revised Manuscript Received November 23, 1999

ABSTRACT: Resonance Raman spectra of native and recombinant analogues of oat phytochrome have been obtained and analyzed in conjunction with normal mode calculations. On the basis of frequency shifts observed upon methine bridge deuteration and vinyl and C_{15}-methine bridge saturation of the chromophore, intense Raman lines at 805 and 814 cm^{-1} in P_r and P_{fr}, respectively, are assigned as C_{15}-hydrogen out-of-plane (HOOP) wags, lines at 665 cm^{-1} in P_r and at 672 and 654 cm^{-1} in P_{fr} are assigned as coupled C═C and C−C torsions and in-plane ring twisting modes, and modes at ∼1300 cm^{-1} in P_r are coupled N−H and C−H rocking modes. The empirical assignments and normal mode calculations support proposals that the chromophore structures in P_r and P_{fr} are C_{15}-Z,syn and C_{15}-E,anti, respectively. The intensities of the C_{15}-hydrogen out-of-plane, C═C and C−C torsional, and in-plane ring modes in both P_r and P_{fr} suggest that the initial photochemistry involves simultaneous bond rotations at the C_{15}-methine bridge coupled to C_{15}−H wagging and D-ring rotation. The strong nonbonded interactions of the C- and D-ring methyl groups in the C_{15}-E,anti P_{fr} chromophore structure indicated by the intense 814 cm^{-1} C_{15} HOOP mode suggest that the excited state of P_{fr} and its photoproduct states are strongly coupled.

Plants sense the quality and quantity of light in their environment and alter their patterns of growth and development to better exploit their surroundings (*1*). These light-driven adaptations are controlled by several photoreceptors including the biliprotein phytochrome (*2*). Phytochrome isolated from etiolated oat seedlings (*Avena sativa*) is a water-soluble protein dimer of 124 kDa subunits (*3*). Each subunit contains a thioether-linked 2,3-dihydrobiliverdin prosthetic group called phytochromobilin (*4*). Phytochrome exists in one of two photointerconvertible forms: P_r,[1] which preferentially absorbs light in the red (λ_{max} = 665 nm) region of the visible spectrum; and P_{fr}, which absorbs light in the far-red region (λ_{max} = 730 nm). The incident light controls the P_r:P_{fr} steady-state ratio, and the plant responds via a molecular mechanism that is currently the subject of intense research (*5*−*7*).

The chromophore structure in phytochrome has been examined with resonance Raman (RR) spectroscopy because this method provides a sensitive in situ structural probe of the photoreaction mechanism. Raman vibrational spectra of phytochrome have been obtained using methods such as preresonant excitation (*8, 9*), shifted-excitation Raman difference spectroscopy (SERDS) (*10*), Fourier transform Raman spectroscopy (*11*), surface-enhanced RR spectroscopy (*12, 13*), and Soret band excitation (*14*−*16*). The consensus of these studies is that the geometry of the methine bridge between the C and D rings of phytochromobilin is C_{15}═C_{16} Z in P_r and C_{15}═C_{16} E in P_{fr}. However, despite this extensive previous work, normal mode assignments of the vibrational bands of P_r and P_{fr} have been limited to examinations of recombinant phytochromopeptides (*17*) and model compounds (*18*−*21*).

Since the first resonance Raman spectra of P_r and P_{fr} were reported (*8, 9*), the prominent lines in these spectra at ∼800 cm^{-1} have been the subject of interest and investigation. Frequency considerations suggest that these modes can be due to C−H, N−H, and/or C═O out-of-plane wagging, ring breathing, and/or methyl stretching vibrations. Based on deuterium exchange experiments, it was found that these modes were not due to N−H wagging vibrations, and it was therefore suggested that they were due to C−H out-of-plane

† This work was supported by NSF Grants CHE 9801651 to R.A.M. and MCB96-04511 to J.C.L. J.A.H. was supported in part by a Howard Hughes Summer Honors Advance Research Program fellowship for undergraduate research.

* To whom correspondence should be addressed.

‡ University of California, Berkeley.

§ Present address: Lawrence Berkeley National Laboratory, 1 Cyclotron Rd., Berkeley, CA 94720.

|| University of California, Davis.

⊥ Present address: Department of Molecular Biology, The Scripps Research Institute, 10550 N. Torrey Pines Rd., La Jolla, CA 92037.

Present address: Department of Biochemistry, University of Wisconsin, Madison, WI 53705.

▽ University of Leiden.

[1] Abbreviations: d-BV, deuterated biliverdin IXα; DMSO, dimethyl sulfoxide; DP-dme, deuterioporphyrin-IX dimethyl ester; *d*-heme, hemin-D_4; DTT, dithiothreitol; EDTA, ethylenediaminetetraacetate; EGTA, ethylene glycol bis(β-aminoethyl ether)-*N*,*N*,*N*′,*N*′-tetraacetic acid; EPPS, *N*-(2-hydroxyethyl)piperazine-*N*′-3-propanesulfonic acid; HOOP, hydrogen out-of-plane; P_r, the red-light absorbing form of phytochrome; P_{fr}, the far-red-light absorbing form of phytochrome; PCB, phycocyanobilin phytochrome; PEB, phycoerythrobilin phytochrome; PΦB, phytochromobilin phytochrome; d-PΦB, $C_{5,10,15}$-d_3-deuterated phytochromobilin phytochrome; RR, resonance Raman.

10.1021/bi991688z CCC: $19.00
Published on Web 02/15/2000

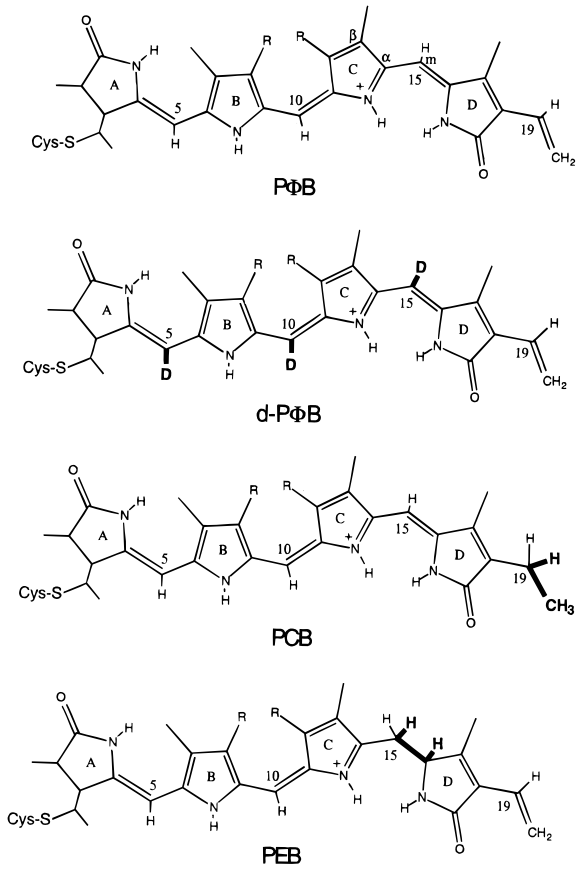

FIGURE 1: Molecular structures of phytochromobilin (PΦB), $C_{5,10,15}$-d_3-phytochromobilin (d-PΦB), phycocyanobilin (PCB), and phycoerythrobilin (PEB). Differences with respect to the PΦB structure have been highlighted.

wagging modes (*9*). The unusual prominence of the modes at ~800 cm^{-1} in the phytochrome RR spectrum indicates that they are important marker bands related to the structure and excited-state geometry changes of the tetrapyrrole chromophore. Analogously intense hydrogen out-of-plane (HOOP) modes in the RR spectra of retinal polyenes have been very important in developing an understanding of rhodopsin photochemistry (*22, 23*).

To more fully elucidate the chromophore and vibrational structure in P_r and P_{fr}, we have obtained RR spectra of full-length 124 kDa recombinant oat phytochromes assembled with its natural chromophore, phytochromobilin (PΦB), and three analogues: phycocyanobilin (PCB), phycoerythrobilin (PEB), and $C_{5,10,15}$-d_3-deuterated phytochromobilin (d-PΦB). The chromophore structures are presented in Figure 1. These analogues were chosen because they readily assemble with recombinant apophytochrome (*24*). By comparing the RR spectrum of native phytochrome with that of its deuterated derivative and the analogues saturated at the C_{15}═C_{16} (PEB) and C_{19}═C_{20} (PCB) positions, we have assigned the vibrational spectra of the P_r and P_{fr} chromophores. These studies coupled with vibrational normal mode calculations demonstrate that the intense Raman bands of P_r and P_{fr} at ~800 cm^{-1} are C−H out-of-plane vibrations and, more specifically, that the bands at 805 cm^{-1} in P_r and at 814 cm^{-1} in P_{fr} are C_{15}−H wagging modes. Furthermore, the bands at ~665 cm^{-1} are best assigned as C═C torsional modes mixed with C−H wagging and C- and D-ring in-plane rotation modes. This analysis confirms that the chromophore structure of phytochrome is C_{15}-Z,syn in P_r and C_{15}-E,anti in P_{fr} and supports the C_{10}-E,anti chromophore geometry (*10, 25*). The observation of RR-active C═C torsional, HOOP, and ring modes confirms that the initial excited-state reaction dynamics involve C_{15}═C_{16} isomerization and indicates that the C−H wagging and in-plane ring modes also contribute to the intrinsic reaction coordinate. This suggests that the isomerization in P_r and especially in P_{fr} is driven by the intramolecular nonbonded steric interaction of substituents on the C and D rings. In this sense, the reaction mechanism in phytochrome is analogous to that in rhodopsin where nonbonded interactions play a significant role in the initial isomerization dynamics (*26*).

EXPERIMENTAL PROCEDURES

Phytochrome Expression, Assembly, and Purification. Recombinant oat apophytochrome A was expressed in yeast strain pMASPHYA/29A, assembled with the desired bilin, and purified as described previously (*27*). Prior to RR spectroscopy, purified recombinant phytochromes were transferred into TEGE buffer (25 mM Tris-HCl, pH 8.0, 25% ethylene glycol, 1 mM EDTA, 1 mM DTT) using a Millipore Ultrafree spin filter (MWCO 100 kDa), and stored at −80 °C. Native phytochrome was isolated as described previously (*28*).

Bilin Preparation. Phycocyanobilin PCB was prepared from lyophilized *Spirulina platensis* (Sigma) (*29*). The PΦB and PEB were prepared by methanolysis of acetone-treated *Porphyridium cruentum* cells (*30*). These three bilins were purified by HPLC and their concentrations determined optically (*24*). The d-PΦB was prepared from meso-deuterated hemin; the details of the synthesis will be found in the Supporting Information. The assembled d-PΦB was characterized by evaluation of the visible spectra of P_r and P_{fr}. The d-PΦB was photointerconvertible between the P_r and P_{fr} forms with wavelength maxima at 664 and 726 nm, respectively. The photoconversion properties and visible spectra of d-PΦB were nearly identical to those of native phytochrome.

Resonance Raman Spectra. To obtain RR spectra of the P_r form of phytochrome, samples in 50 mM EPPS, pH 8.0, 1 mM EDTA buffer were placed in a 1.4 mm i.d. glass capillary. Spectra were acquired using 30 mW of 740 nm excitation for the native, PΦB, and PCB phytochromes and 40 mW of 710 nm excitation for the PEB phytochrome. Since some buffer vibrational bands were equivalent in intensity to the phytochrome bands, spectra of the buffer solution were also acquired and subtracted from the RR spectra of the recombinant phytochromes. Raman scattered light was collected 90° from the incident probe beam and focused onto a 200 μm slit of a Spex 1401 spectrograph equipped with CCD detection. The data were corrected for the spectral sensitivity of the detection system using a calibrated tungsten lamp (EG&G model 590-20).

For the P_{fr} RR experiments, phytochrome was dialyzed into 50 mM EPPS, pH 8.0, 1 mM EDTA buffer and then concentrated to ~20 μM using Centricon-100 microconcentrators (Amicon). To acquire spectra, the 75 μL sample was loaded into a microspinning cell described previously (*31*) and rotated (500 rpm) while spatially separated probe (750 nm) and recycling beams (647 nm) were used to maintain phytochrome in the P_{fr} form. The 750 nm (2 mW) Ti:sapphire

probe beam was focused on the sample using a 75 mm spherical lens to a diameter of 0.5 mm while the 647 nm (15 mW) recycling beam from a Spectra-Physics 2025 krypton ion laser was directed onto the sample with a spot size of approximately 4 mm. The recycling beam was focused approximately 8 mm from the center of the cell on the side opposite the probe beam. Under these conditions, the conversion of P_{fr} to photoproduct by the probe beam depends on the photoalteration parameter: $F = (3.824 \times 10^{-21})P\epsilon\phi/\nu d$ (*32*). For the P_{fr} experiments [$\epsilon_{750} = 60\,000$ M^{-1} cm^{-1}, $\phi = 0.069$ (*33*), $\nu = 43$ cm/s, and $d = 0.5$ cm], we calculate that $F = 0.004$. This means that less than 0.4% of the P_{fr} molecules that rotate through the probe laser beam will be photoconverted in one pass.

RR spectra of phytochrome were acquired using the shifted-excitation Raman difference spectroscopy (SERDS) technique (*25, 34*) because it facilitates Raman spectral acquisition when there is a strong fluorescence background. With this technique, two Raman spectra are obtained with excitation frequencies shifted by 10 cm^{-1} relative to one another but with all other experimental conditions identical. The difference of these two spectra yields a SERDS spectrum. Derivative features, corresponding to Raman lines, are then fit to a model which assumes that the bands in the Raman spectrum are a difference of Gaussian peaks. The amplitude, position, and width of each peak are determined via nonlinear least-squares fit, and these parameters are then used to generate the Gaussian peaks representing the Raman spectrum.

Vibrational Calculations. To aid in the interpretation of the phytochrome RR spectra, vibrational calculations were performed using the QCFF-π method *(35)* as previously described (*25)*. The geometries were minimized and vibrational frequencies and intensities calculated for the $C_5{=}C_6$-Z, $C_4{-}C_5$-anti, $C_{10}{=}C_{11}$-E, $C_9{-}C_{10}$-anti, and $C_{15}{=}C_{16}$-Z, $C_{14}{-}C_{15}$-syn (P_r) or $C_{15}{=}C_{16}$-E, $C_{14}{-}C_{15}$-anti (P_{fr}) chromophore structures of PΦB, d-PΦB, and PCB, and the P_r chromophore structure of PEB.

RESULTS

Experimental Assignment of Phytochrome Normal Modes

The integrated SERDS spectra of the P_r and P_{fr} analogues along with the native phytochrome RR spectra are presented in Figures 2 and 3. The experimental SERDS spectra used to obtain the integrated SERDS spectra may be found in the Supporting Information. These spectra exhibit prominent RR difference bands in the frequency range from 400 to 1700 cm^{-1}. The similarity in shape, intensity, and position of the bands in the native and recombinant P_r and P_{fr} RR spectra indicates that the holo and PΦB recombinant proteins contain a chromophore with the same structure and environmental tertiary interactions consistent with previous studies (*27*). This strongly suggests that the recombinant phytochrome protein chromophore domain is folded into the same structure as the native protein isolated from oats. The spectra correspond very well with previously published P_r and P_{fr} Raman spectra (*9, 10*). However, there are some differences with respect to the spectra presented by Hildebrandt et al. *(11)* which suffer from incomplete subtraction of interfering buffer components. Although the peak positions and frequencies of P_r and P_{fr} agree well with those published by Matysik et al. *(35)*, the peak intensities vary due to their use of 1064 nm Raman excitation which enhances *A*- and *B*-term modes almost equally compared to our resonant conditions which would selectively enhance *A*-term modes (*37*).

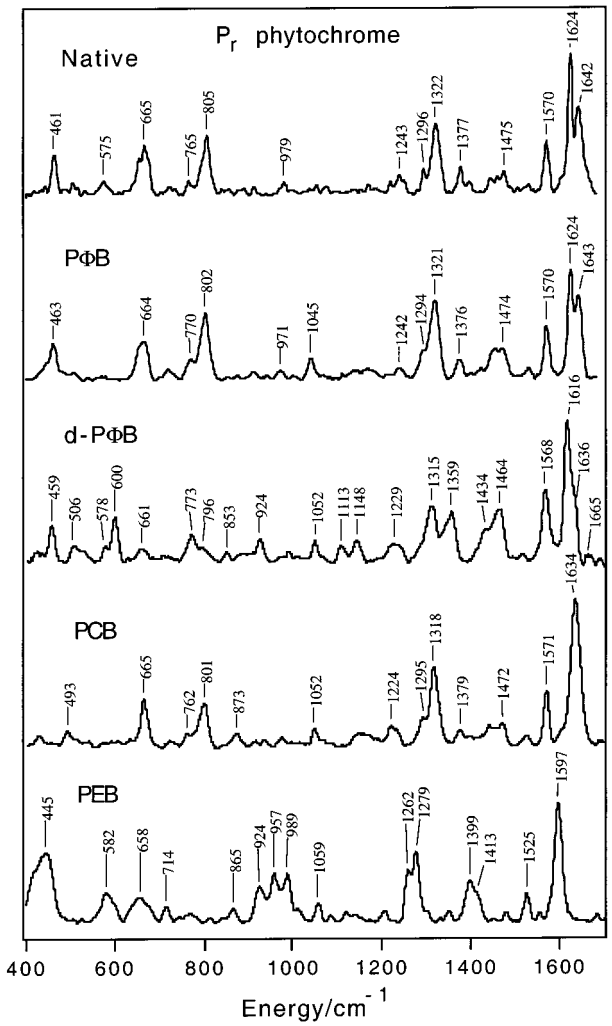

FIGURE 2: Integrated SERDS spectra of the P_r forms of the native (100 μM) and PΦB (25 μM), d-PΦB (25 μM), PCB (25 μM), and PEB (30 μM) recombinant phytochrome chromophore analogues obtained using 740 nm excitation.

Comparison of the integrated P_r SERDS spectra of the PΦB, d-PΦB, PCB, and PEB analogues presented in Figure 2 shows that there are significant similarities as well as differences in their vibrational structure. The bands in the C═C and C═N stretching region of PΦB at 1643, 1624, and 1570 cm^{-1} are replaced by bands at 1636, 1616, and 1568 cm^{-1} in the d-PΦB spectrum, bands at 1634 and 1571 cm^{-1} in the PCB spectrum, and bands at 1597 and 1525 cm^{-1} in the PEB spectrum. The bands at 1376, 1321, 1294, and 1242 cm^{-1} in the N−H and C−H rocking region of the PΦB spectrum are replaced by bands at 1359, 1315, and 1229 cm^{-1} in the spectrum of d-PΦB and bands at 1379, 1318, 1295, and 1224 cm^{-1} in the PCB spectrum. The rocking bands are found at 1413, 1399, 1279, and 1262 cm^{-1} in the spectrum of PEB. The bands at 802 and 770 cm^{-1} in the hydrogen out-of-plane wagging region of PΦB are replaced by much weaker modes at 796 and 773 cm^{-1} in the d-PΦB spectrum whereas the PCB spectrum has somewhat weaker modes at 801 and 762 cm^{-1}, and the PEB spectrum exhibits a strikingly different pattern with modes at 989, 957, 924,

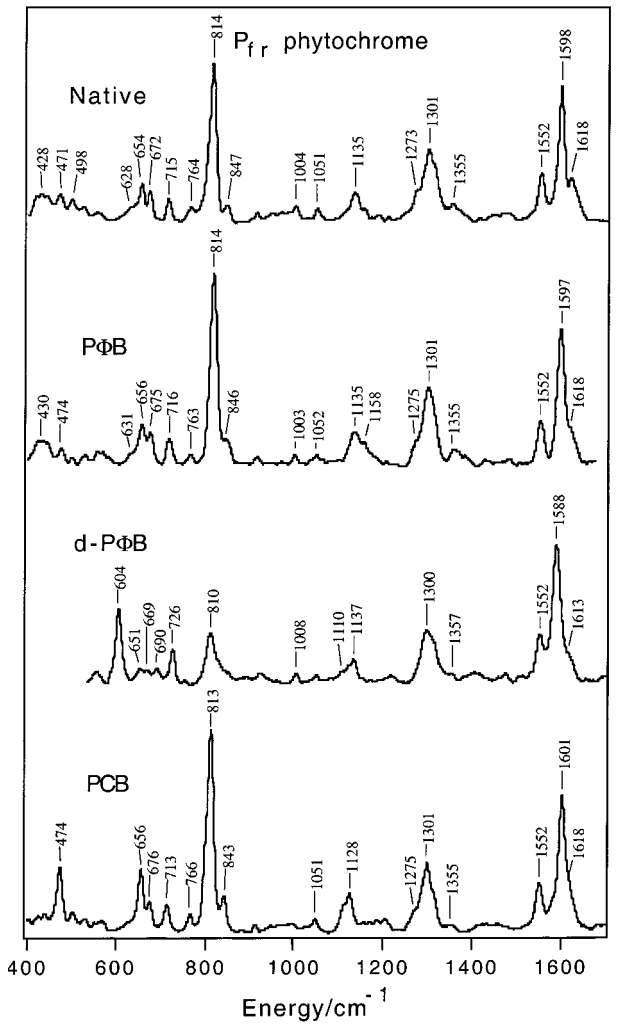

FIGURE 3: Integrated SERDS spectra of the P_{fr} forms of the native (75 μM) and PΦB (20 μM), d-PΦB (20 μM), and PCB (20 μM) recombinant phytochrome chromophore analogues obtained using 750 nm excitation.

and 865 cm^{-1}. The low wavenumber region of PΦB is characterized by modes at 664 and 463 cm^{-1}. Modes occur at 661, 600, 578, 506, and 459 cm^{-1} in the spectrum of d-PΦB, at 665 and 493 cm^{-1} in the spectrum of PCB, and at 714, 658, 582, and 445 cm^{-1} in the spectrum of PEB.

The integrated P_{fr} phytochrome analogue SERDS spectra are presented in Figure 3. The C═C and C═N stretching region of the PΦB analogue has peaks at 1597 and 1552 cm^{-1} with a shoulder at 1618 cm^{-1}. Similar bands appear at 1613 (sh), 1588, and 1552 cm^{-1} in the spectrum of d-PΦB and at 1618 (sh), 1601, and 1552 cm^{-1} in the spectrum of PCB. In the N−H and C−H rocking region, the PΦB spectrum exhibits modes at 1355, 1301, and 1275 cm^{-1}, the d-PΦB spectrum exhibits modes at 1357 and 1300 cm^{-1}, and in the PCB spectrum these modes are found at 1355 and 1301 cm^{-1} with a shoulder at 1275 cm^{-1}. The C−C and C−N stretching regions of PΦB and d-PΦB spectra both have similar small bands at ∼1137 cm^{-1}, but the PCB spectrum has bands centered at 1128 cm^{-1}. In the hydrogen out-of-plane wagging region, the spectrum of PΦB has modes at 846, 814, 763, and 716 cm^{-1}, the spectrum of d-PΦB has bands at 810 and 726 cm^{-1}, and the spectrum of PCB has bands at 843, 813, 766, and 713 cm^{-1}. The low-wavenumber region of PΦB is characterized by bands at 675 and 656 cm^{-1} whereas the d-PΦB spectrum has weak bands at 690, 669, and 651 and a strong band at 604 cm^{-1}. The region below 500 cm^{-1} in the d-PΦB SERDS spectrum was obscured by strong Rayleigh scattering. The low-wavenumber region of PCB has bands at 676, 656, and 474 cm^{-1}.

Methine Bridge Deuterium Substitution. The d-PΦB analogue has all methine bridge protons replaced with deuterium. Based on a harmonic oscillator model, we expect that modes exhibiting C−D vibrational character will shift to lower frequency, thereby allowing qualitative assignment. For the P_r spectra in Figure 2, we observe that the 1636, 1616, and 1568 cm^{-1} C═C and C═N modes of d-PΦB have shifted down −7, −8, and −2 cm^{-1}, respectively, from the corresponding frequencies in PΦB, indicating that these modes have some methine bridge C−H rocking character. The lack of significant shifting of the 1570 cm^{-1} mode supports its previous assignment as a localized $C{=}NH^+$ stretching mode (*9*, *10*).

The 1300 cm^{-1} C−H and N−H rocking region is very sensitive to C−D methine bridge isotopic substitution. The spectrum of the d-PΦB analogue has a band at 1315 cm^{-1} with similar intensity to the 1321 cm^{-1} band of the PΦB analogue spectrum. However, there is a line with increased intensity at 1359 cm^{-1} in the d-PΦB spectrum which may correspond to the 1376 cm^{-1} line in the PΦB spectrum. Modes near 1375 cm^{-1} have been assigned to C−N and C−C stretching vibrations in porphyrins (*38*, *39*). This is confirmed by our QCFF-π calculations which predict that these modes occur at ∼1410 cm^{-1}. The modes observed at ∼1375 cm^{-1} in the P_r spectra must be C−N and $C_\alpha-C_m$ stretching vibrations whose frequencies are altered in d-PΦB because they are coupled with C−H(D) vibrations. The band at 1229 cm^{-1} shifts down from 1242 cm^{-1}, showing that it also has C−H(D) character. There are two new lines at 1148 and 1113 cm^{-1} in the d-PΦB spectrum that are assigned as C−D rocking bands shifted down from the 1300 cm^{-1} region. Based on the reduced mass of a pure C−D vibration, we expect to observe a C−D rock at ∼1000 cm^{-1} if the C−H counterpart is observed at ∼1350 cm^{-1} (*40*). QCFF-π calculations predict that C−D rocking modes in tetrapyrroles should occur at ∼1130 cm^{-1} mixed with C−C stretches (see below), in good agreement with the 1113 and 1148 cm^{-1} frequencies observed in d-PΦB. The band at 924 cm^{-1} in the spectrum of d-PΦB is also a candidate for a C−D rocking mode.

We observe marked shifts in the 800−850 cm^{-1} C−H(D) out-of-plane wagging region upon bridge deuteration. The mode at 802 cm^{-1} in the PΦB spectrum is replaced by weaker bands at 773 and 796 cm^{-1}. These bands may be residual C−H wags due to incomplete deuterium substitution of the d-PΦB analogue or exchange of the C_5-D for C_5-H during assembly (*4*), or they could be modes with no C−H(D) vibrational character that occur at ∼770 cm^{-1} in PΦB. The 802 cm^{-1} band, tentatively assigned as a hydrogen out-of-plane vibration by Fodor et al. (*9*), has shifted down to 600 cm^{-1} in the d-PΦB spectrum. We base this assignment on the larger reduced mass that is expected to lower this frequency by ∼200 cm^{-1} (*40*). Additional evidence is provided by QCFF-π calculations which predict C−D wagging modes at ∼660 cm^{-1} for d-PΦB and at ∼870 cm^{-1} for their C−H counterparts (a shift of −210 cm^{-1}). We therefore assign the 802 cm^{-1} P_r band of native phytochrome

as a methine bridge HOOP wagging mode.

The modes centered at 664 cm^{-1} in the spectrum of PΦB have been previously observed but not assigned (*9, 10, 36*). Either they have lost intensity and are still centered at 661 cm^{-1} or they are shifted down to ~506 cm^{-1} in the d-PΦB spectrum of P_r. The shifts indicate that these modes are significantly coupled to the methine bridge C−H vibrational coordinates; in this case, they would be best assigned as methine bridge torsions and/or ring modes. The mode at 463 cm^{-1} in the spectrum of PΦB probably corresponds to the mode observed at 459 cm^{-1} in the d-PΦB spectrum.

The P_{fr} spectra of PΦB and d-PΦB in Figure 3 also exhibit informative shift patterns. The −5 and −9 cm^{-1} shifts of the 1618 and 1597 cm^{-1} modes upon bridge deuteration in d-PΦB indicate that these modes have some C−H(D) vibrational character. The lack of shift of the 1552 cm^{-1} band indicates that this is a localized C═NH^+ stretching mode consistent with its previous assignment (*9, 10*). There are no significant changes in the C−H and N−H rocking region upon methine bridge deuterium substitution, indicating that the observed modes at ~1300 cm^{-1} do not involve methine C−H displacements. The intense 814 cm^{-1} band in the hydrogen out-of-plane wagging region of the PΦB spectrum is replaced by a weaker and broader band at 810 cm^{-1} in the d-PΦB spectrum. The prominent new C−D mode of d-PΦB appears at 604 cm^{-1}. Based on the same arguments used in making the HOOP assignment for P_r, we assign the band at 814 cm^{-1} in P_{fr} as a HOOP wag. The modes observed at ~810 cm^{-1} in the d-PΦB-P_{fr} spectrum may be due to C−H wags from incomplete deuterium substitution, or they could be modes with no C−H(D) vibrational character. The mode at 716 cm^{-1} in the PΦB spectrum apparently shifts up to 726 cm^{-1} in the d-PΦB spectrum, indicating that this mode is weakly coupled to the C−H(D) vibrations. The modes at 631, 656, and 675 cm^{-1} in the spectrum of PΦB are replaced by very weak modes at 651, 669, and 690 cm^{-1} in the spectrum of d-PΦB. These modes may have lost intensity or shifted as a result of coupling to C−H(D) displacements. The modes at 656 and 675 cm^{-1} in the PΦB spectrum are therefore candidates for methine bridge torsions and/or ring modes.

D-Ring Vinyl Saturation. The spectra of the PCB adduct are useful because the modes observed in PΦB spectra involving C_{19}═C_{20} vibrational character are altered due to the saturation of the C_{19}═C_{20} double bond. In the C═C and C═N stretching region, the PCB analogue spectrum of P_r has a mode centered at 1634 cm^{-1} and another mode at 1571 cm^{-1}. The 1624 cm^{-1} mode in the PΦB spectrum apparently shifts to 1634 cm^{-1} in the PCB analogue spectrum, as postulated by Kneip et al. (*17*) in a study of recombinant phytochromopeptides. This shift is consistent with a less conjugated structure because the force constant for stretching increases with decreasing conjugation. The 1624 cm^{-1} mode must therefore contain significant C_{19}═C_{20} stretching character. The upshifted 1634 cm^{-1} band of PCB then overlaps with the 1643 cm^{-1} band. The stationary 1570 cm^{-1} C═NH^+ stretching band has no vinyl character. The 1200−1400 cm^{-1} N−H and C−H rocking regions of the PΦB and PCB P_r spectra are very similar. The shift of the 1242 cm^{-1} band in PΦB to 1224 cm^{-1} in PCB indicates that this mode has some vinyl character. The bands at 802 and 770 cm^{-1} in the PΦB spectrum are replaced by slightly weaker bands at 801 and 762 cm^{-1} in the PCB spectrum. The mode at 463 cm^{-1} in the PΦB spectrum does not appear in the PCB spectrum, indicating that this mode involves primarily the C_{19}═C_{20} vinyl group and may be a C_{19}═C_{20} torsional mode.

Few spectroscopic shifts are observed upon C_{19}═C_{20} saturation in the P_{fr} spectra (Figure 3). The modes at 1618, 1597, and 1552 cm^{-1} in the PΦB spectrum shift very little in the PCB spectrum, indicating that these modes have little or no vinyl character. The N−H and C−H rocking region shows no significant shifts upon C_{19}═C_{20} saturation. The modes observed at ~1136 cm^{-1} in the PΦB spectrum appear at 1128 cm^{-1} in the PCB spectrum, indicating that they contain some vinyl character. The C−H wagging regions of PΦB and PCB are virtually identical. The PΦB modes at 656 and 675 cm^{-1} are roughly equal in intensity whereas the corresponding 656 cm^{-1} mode in PCB has gained intensity relative to the 676 cm^{-1} mode. This indicates that the 656 cm^{-1} mode has some vinyl character. Surprisingly, a moderately intense mode appears at 474 cm^{-1} in the PCB-P_{fr} spectrum. This may occur because modes centered at ~430 cm^{-1} in PΦB-P_{fr} shift to overlap with the weak mode at 474 cm^{-1} in PΦB.

C_{15}═C_{16} Methine Bridge Saturation. The PEB analogue differs from the PΦB chromophore by saturation of the C_{15}═C_{16} double bond. The Raman spectrum of the PEB analogue is very useful because the reactive modes associated with initial C_{15}═C_{16} isomerization are lost. Limited proteolysis studies and electronic absorption spectroscopy (*41*) have indicated that the PEB analogue has a locked P_r structure. This adduct has a fluorescence quantum yield >0.75, which confirms its lack of photochemical internal conversion and reactivity (*42*). Additionally, the majority of the $\pi-\pi$ conjugation is confined to the B- and C-ring moieties, and we expect to observe resonant vibrational scattering primarily from this part of the molecule. The spectrum of PEB in Figure 2 has a very different vibrational structure compared to that of the spectrum of PΦB. The characteristic C═C and C═N modes of PΦB are replaced by modes at 1597 and 1525 cm^{-1}. There are modes at 1413, 1399, 1279, and 1262 cm^{-1} which are probably C−H and N−H rocking and C−C and C−N stretching modes. Modes are observed in the C−C stretching region at 989, 957, 924, and 865 cm^{-1} in the PEB spectrum. It is important to note that the PEB spectrum lacks C═C and C═N modes above 1600 cm^{-1}, N−H rocking modes at ~1320 cm^{-1}, and HOOP modes at ~800 cm^{-1} that are characteristically observed in the PΦB spectrum.

Calculation of Normal Modes for Phytochrome

Vibrational calculations were performed for the PΦB, d-PΦB, PCB, and PEB chromophore structures of P_r and P_{fr}, respectively. Although QCFF-π is a low-level quantum mechanical procedure, it has been used to successfully predict normal modes of similar systems such as rhodopsin and retinal, and it has shown good correspondence to higher level MNDO calculations (*22, 26, 43*). The results of these calculations are summarized in Figures 4 and 5. The correlation diagrams show that the P_r and P_{fr} chromophore structures exhibit characteristic frequency shifts upon methine bridge deuteration, vinyl saturation, and methine bridge saturation. Although the absolute frequencies in the calculations do not correspond precisely with the Raman spectra,

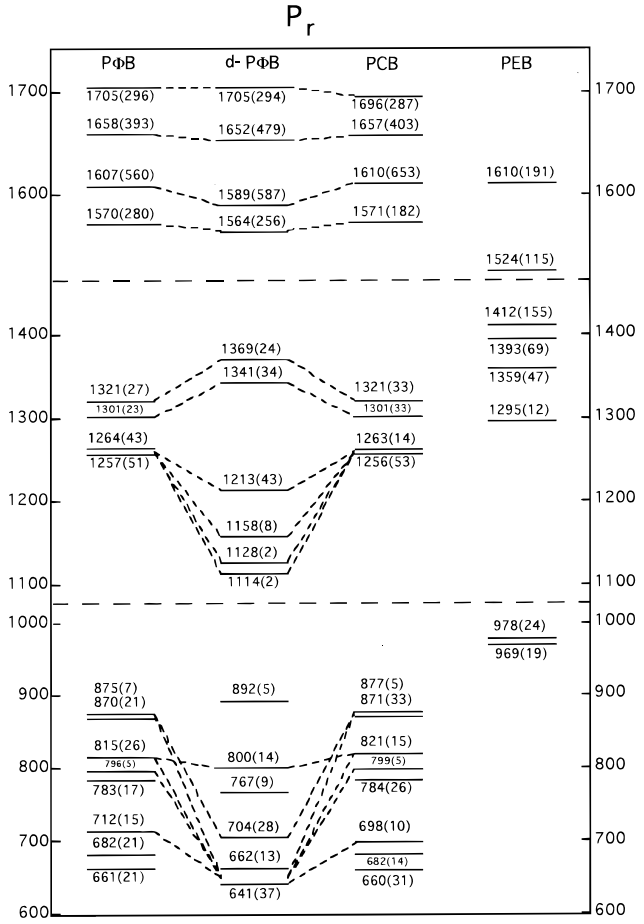

FIGURE 4: Correlation diagram of the calculated vibrational frequencies for the PΦB, d-PΦB, PCB, and PEB C_{15}-Z,syn P_r phytochrome chromophore. Relative RR intensities of each mode are given in parentheses.

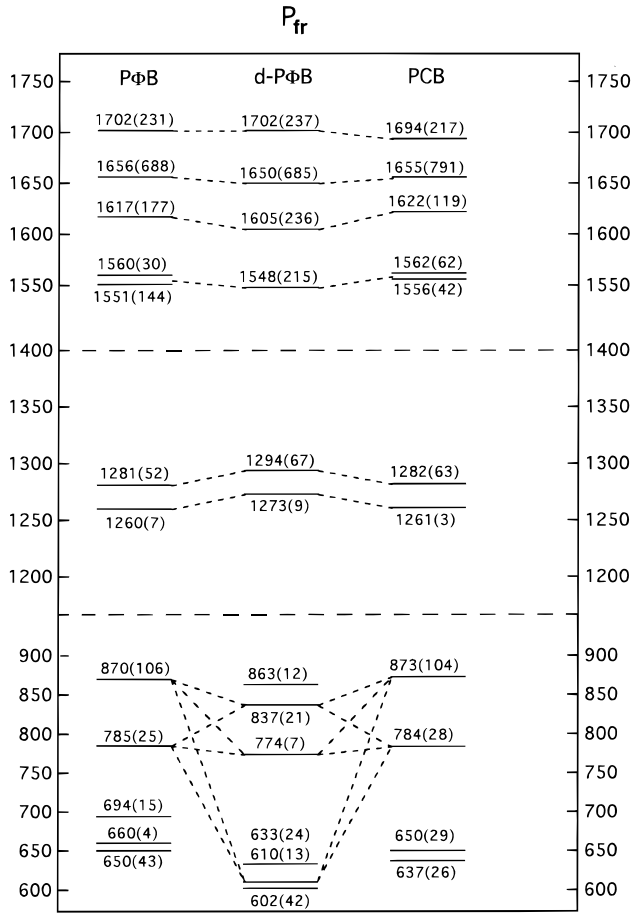

FIGURE 5: Correlation diagram of the calculated vibrational frequencies for the PΦB, d-PΦB, and PCB C_{15}-E,anti P_{fr} phytochrome chromophore. Relative RR intensities of each mode are given in parentheses.

the frequency ordering and qualitative frequency shifts show reasonable correspondence with the changes observed in the analogue spectra. We will now qualitatively compare the predicted frequency shifts for the analogues with the experimental spectra and make some inferences about the normal mode character of the bands.

Ethylenic Stretching Region. The ethylenic region of P_r phytochrome is predicted to undergo minor band shifts upon deuterium substitution and vinyl saturation and more dramatic changes upon C_{14}═C_{15} saturation. Briefly, the P_r vibrational calculations for PΦB predict four intense modes in the C═C and C═N stretching region at 1705, 1658, 1607, and 1570 cm^{-1}. These modes are calculated at 1705, 1652, 1589, and 1564 cm^{-1} for d-PΦB and at 1696, 1657, 1610, and 1571 cm^{-1} for PCB. Only two modes are calculated in this region at 1610 and 1524 cm^{-1} for PEB. The calculations summarized in Figure 4 are in reasonable agreement with the spectra in Figure 2. However, the 1705 cm^{-1} mode of PΦB involving C═O, C_{17}═C_{18}, and vinyl stretching and N−H rocking vibrations of the D ring has no obvious intense counterpart in the Raman spectra. The calculated 1658 and 1607 cm^{-1} modes of PΦB are dominated by C_{10}═C_{11}, C_{14}═N, and C_{15}═C_{16} stretching coupled to N(C)−H and $C_{10,15}$−H rocking vibrations. The frequency of these modes shifts down in the case of $C_{10,15}$−D substitution where C−D rocking replaces C−H rocking. This is consistent with the Raman spectra where we observe small shifts of the ethylenics at 1643 and 1624 cm^{-1} in PΦB to 1636 and 1616 cm^{-1} in d-PΦB, indicating that the experimentally observed modes contain C−D rocking character. The 1607 cm^{-1} PΦB mode is predicted to shift 3 cm^{-1} to 1610 cm^{-1} in PCB-P_r. However, the magnitude of this shift does not correspond well with the shift of the 1624 cm^{-1} band in PΦB to ∼1634 cm^{-1} in PCB. This shift was also experimentally observed by Kneip et al. (*17*). The calculated ethylenic modes of PEB at 1610 and 1524 cm^{-1} exhibit no correlation with those of the other chromophores. The predicted lower frequency ethylenic modes are very consistent with the two ethylenic modes observed for PEB at 1597 and 1525 cm^{-1}. In general, the calculations are consistent with the hypothesis that ethylenic stretching is coupled to N−H and C−H rocking, and that methine bridge deuteration shifts mixed ethylenic and C−D rocking modes to slightly lower frequency.

The calculations summarized in Figure 5 for P_{fr} phytochrome are in reasonable agreement with the spectra in Figure 3. As with P_r, the 1702 cm^{-1} mode finds no corresponding band in the experimental spectra. The calculated 1656 and 1617 cm^{-1} ethylenic modes of PΦB shift down to 1650 and 1605 cm^{-1} for d-PΦB, consistent with the observed pattern where bands at 1618 and 1597 cm^{-1} in PΦB shift down −5 and −9 cm^{-1}, respectively. This is similar to the case for P_r where deuterium substitution results in lower frequency ethylenics due to their mixed C═C and C−H(D) character. The most intense calculated ethylenic

line shifts up slightly in PCB, which is not inconsistent with the observed 4 cm^{-1} upshift of the ethylenic band. It is important to note that for both P_r and P_{fr}, the experimentally observed C═NH^+ modes at 1570 and 1552 cm^{-1}, respectively, are predicted at 1570 and 1551 cm^{-1} and the calculations also indicate that they are strongly coupled to N−H rocking modes *(10)*.

C−N and C−C Stretching and H-Rocking Region. Four modes are calculated to occur for P_r in this region at 1321, 1301, 1264, and 1257 cm^{-1}. These are split into two higher frequency mixed C−C and C−N stretching and N−H rocking modes at 1369 and 1341 cm^{-1} and four lower frequency mixed C−D and N−H rocking modes at 1213, 1158, 1128, and 1114 cm^{-1} in d-PΦB. The calculated 100−150 cm^{-1} frequency lowering of the C−H rocks upon deuterium substitution is in excellent agreement with the observed 1113 and 1148 cm^{-1} modes of the d-PΦB RR spectrum in Figure 2. Also in the RR spectra, intensity may shift from 1321 cm^{-1} to a band at 1359 cm^{-1}, consistent with the calculated +40 cm^{-1} shift of the C−C and C−N stretching and N−H rocking modes shown in Figure 4. However, the calculations do not predict the residual intensity observed at 1315 cm^{-1}. This residual intensity may be due to N−H rocking modes that result from exchange (*9*−*11*). For PCB, the calculated modes are virtually identical to the calculated PΦB frequencies, entirely consistent with the lack of significant peak shift observed in the Raman spectra of Figure 4 upon vinyl saturation. For PEB, calculated modes occur at 1412, 1393, 1359, and 1295 cm^{-1} and involve primarily C−C and C−N stretching and N−H and C−H rocking that are delocalized over the B- and C-ring moieties. We cannot draw any direct correspondence between the RR spectra of PEB shown in Figure 2 and the calculated normal modes of PEB. In general, the calculations are consistent with the hypothesis that C−C and C−N stretching is coupled to N−H and C−H rocking, and that methine bridge deuteration shifts C−D rocking modes to lower frequency. We propose that for P_r, the 1376 cm^{-1} mode of PΦB involves C−N stretching as seen in porphyrins (*38*, *39*). The 1321 and 1294 cm^{-1} modes are N−H and C−H rocking modes significantly coupled to C−C and C−N stretching coordinates.

In the H-rocking and C−C and C−N stretching region of P_{fr}, two modes are calculated at 1281 and 1260 cm^{-1} for PΦB. These modes shift to 1294 and 1273 cm^{-1} in d-PΦB and to 1282 and 1261 cm^{-1} in PCB. These modes have the same vibrational character as the 1321 and 1301 cm^{-1} modes calculated for PΦB-P_r except that there are additional C−C and C−N stretching contributions that shift the frequency higher. The calculations show that these modes in P_{fr} are much less sensitive to methine bridge deuteration, consistent with the lack of significant frequency shifts observed experimentally in Figure 3 and entirely consistent with the vibrations at 1300 cm^{-1} being primarily N−H rocking (*9*, *10*). Vinyl substitution also has little impact on the vibrational structure.

Hydrogen-Wagging and Torsional Region. In the H-wagging region of P_r, the calculation predicts that PΦB has mixed $C_{5,10,15}$−H wagging modes at 875 and 870 cm^{-1}. The calculated −200 cm^{-1} shift of intensity from 870 to 662 cm^{-1} for P_r is in good agreement with the 802 to 600 cm^{-1} (−202 cm^{-1}) shift of intensity observed in the RR spectra in Figure 2 upon methine bridge deuteration. Residual intensity is predicted in the region from 767 to 892 cm^{-1} because of C−D rocking coupled to C- and D-ring in-plane rotations, and this is consistent with the bands at 773, 796, and 853 cm^{-1} in the d-PΦB spectrum. Mixed modes of $C_{5,10,15}$−D wagging and C- and D-ring in-plane rotation are calculated to occur at 704 and 641 cm^{-1}, but the 662 cm^{-1} mode is calculated to be mixed C_{15}═C_{16} torsional, C-ring folding, and D-ring in-plane rotation. Therefore, the d-PΦB-P_r bands at 506, 578, and 661 cm^{-1} are probably C−D wagging mixed with C- and D-ring in-plane rotations and methine torsions. The PCB calculation exhibits $C_{5,10,15}$−H wagging modes equivalent to PΦB at 877 and 871 cm^{-1}. PEB exhibits no strong C−H wagging bands but relatively intense C−C stretching modes at 978 and 969 cm^{-1}.

The P_{fr} calculations predict that PΦB has two mixed $C_{5,10,15}$−H wagging modes at 870 and 785 cm^{-1}. In d-PΦB, a calculated −250 cm^{-1} shift of intensity of these modes from 870 to 633 and 610 cm^{-1} for P_{fr} is in good agreement with the 814 to 604 cm^{-1} (−210 cm^{-1}) shift of intensity observed in the RR spectra in Figure 3 upon methine bridge deuteration. PΦB-P_{fr} is predicted to have additional modes at 660 cm^{-1} involving C_{15}−H wagging, C- and D-ring in-plane rotation, and vinyl rocking; and at 650 cm^{-1} involving C_{14}−C_{15} and C_{15}═C_{16} torsion, and $C_{5,10,15}$−H wagging. In d-PΦB, these modes are replaced by a mode at 863 cm^{-1} involving $C_{5,10,15}$−D rocking, C- and D-ring translation, and N(C)−H wagging; a mode at 837 cm^{-1} involving $C_{10,15}$−D wagging and C-ring in-plane rotation; a mode at 774 cm^{-1} involving $C_{5,10}$−D rocking, C_{15}−D wagging, and C- and D-ring in-plane rotation. Also, for d-PΦB, the $C_{5,10,15}$−D wags are shifted down to 633 and 610 cm^{-1} mixed with C-ring swiveling and to 602 cm^{-1} mixed with C-ring in-plane rotation. For PCB, two $C_{5,10,15}$−H wagging modes occur at 873 and 784 cm^{-1} that are equivalent in character to the PΦB modes. The calculations predict vinyl vibrations to occur at 694 cm^{-1} in PΦB, and we observe a mode whose intensity is affected by vinyl saturation at 656 cm^{-1}. In general, the calculations indicate that C−H wagging is coupled to methine C−C and C═C torsion and ring modes, and methine bridge deuteration shifts mixed C−D wagging modes to lower frequency.

DISCUSSION

The RR spectra and analysis of the structural and isotopic phytochrome analogues presented here allow important vibrational assignments to be made for the P_r and P_{fr} chromophores. These vibrational assignments summarized in Figure 6 provide a better understanding of the ground-state chromophore structures of P_r and P_{fr}. The vibrational assignments together with resonance Raman intensities also provide clues about the nature of the excited-state structure and initial photochemical reaction dynamics of the chromophores in P_r and P_{fr}.

Ethylenic Stretching. The ethylenic modes of P_r are delocalized across the D-ring moiety and the C_{15}-methine bridge whereas the ethylenic modes of P_{fr} are not. The P_r ethylenic modes at 1642 and 1624 cm^{-1} each shift upon C−H(D) exchange, vinyl saturation, and C_{15}═C_{16} saturation. This means that these vibrations must involve the C−H, vinyl, and C_{15}═C_{16} nuclei, indicating ethylenic vibrational

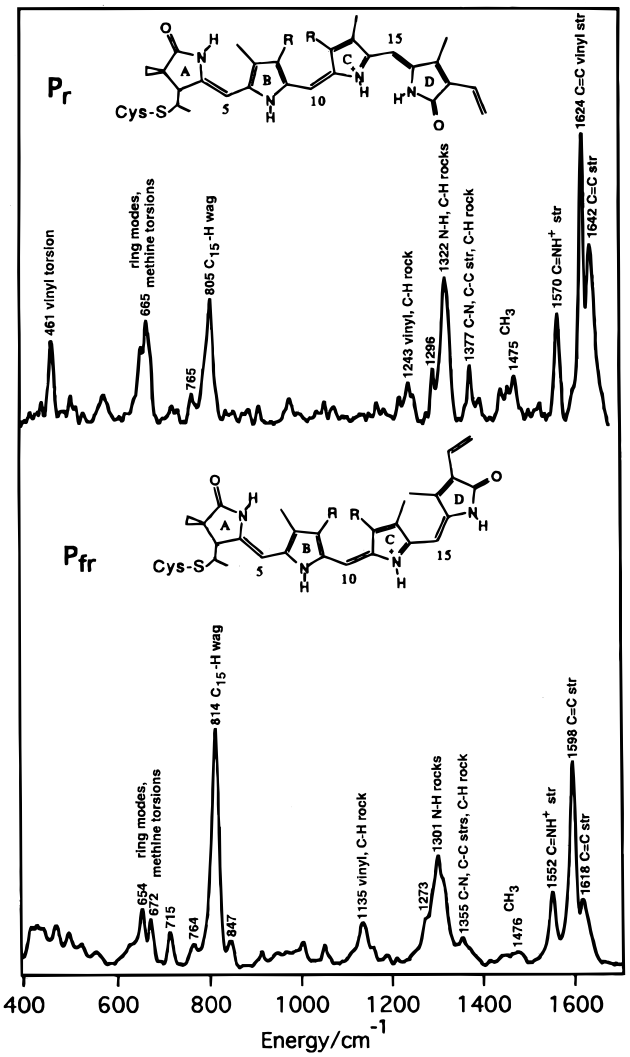

FIGURE 6: Comparison of the resonance Raman spectra of native P_r and P_{fr} phytochromes. Vibrational bands have been labeled with their approximate normal mode character.

delocalization across the D-ring moiety, a conclusion consistent with the calculated vibrational eigenvectors. The P_{fr} ethylenics at 1618 and 1597 cm^{-1} involve C═C stretching that is mixed with just C−H rocking, and these ethylenic modes are not delocalized across the D ring. This conclusion is based principally on the insensitivity of the P_{fr} spectrum to vinyl saturation.

The C═NH^+ stretching modes at 1570 and 1552 cm^{-1} in P_r and P_{fr}, respectively, are localized C═NH^+ modes. Their shift to lower frequencies only with N−H(D) exchange shows that they are primarily C═N stretching mixed with N−H rocking coordinates (*9, 10*). The strong shift induced by isotopic exchange indicates that the C═N groups are all protonated. Based on harmonic oscillator calculations, the degree of shifting of these bands upon N−H(D) exchange may be related to the strength of the C═N bond, changes in the hydrogen bonding environment, or location of the C═N bond in the chromophoric system.

C−N and C−C Stretching and H-Rocking. The modes at 1377 cm^{-1} in P_r and 1355 cm^{-1} in P_{fr} are C−N stretching vibrations mixed with C−C stretching and C−H rocking motions. These modes are sensitive to the C−N bond strength as observed in porphyrins (*44*), but may also be sensitive to the delocalization of π electrons (*45, 46*). These modes are expected to be sensitive to the protonation state and hydrogen-bonding environment of the chromophore as well as to changes in the π bonding structure. The modes at 1322 cm^{-1} in P_r have significant N−H and C−H rocking character whereas the modes at 1301 cm^{-1} in P_{fr} simply involve N−H rocking. Normal mode calculations predict lower N−H vibrational frequencies for the C_{15}-E,anti chromophore in P_{fr} consistent with observation. The modes at ∼1240 cm^{-1} in P_r and ∼1135 cm^{-1} in P_{fr} involve vinyl and C−H rocking motions. Their sensitivity to C−H(D) exchange and vinyl saturation indicates that they are delocalized across the D rings of both P_r and P_{fr}.

C−H Wagging and Torsions. The modes at 805 cm^{-1} in P_r and 814 cm^{-1} in P_{fr} are methine bridge HOOP modes. The fact that the 805 cm^{-1} mode in P_r is absent in the C_{15}═C_{16} saturated PEB analogue strongly suggests that it is a localized C_{15}−HOOP wag. The P_{fr} HOOP mode at 814 cm^{-1} is predicted to contain mixed $C_{5,10,15}$−H wagging character. Modes at ∼665 cm^{-1} in P_r and P_{fr} are mixed HOOPs, methine bridge torsions, and ring rotations. The shifts of these modes with methine bridge deuteration indicate that these modes are significantly mixed with the C−H vibrational coordinates. The mode at 461 cm^{-1} in P_r is a vinyl torsional mode as exemplified by its intensity attenuation with vinyl saturation.

Ground-State Chromophore Structures in P_r and P_{fr}. By comparison of native phytochrome spectra to normal mode calculations and mode assignments based on N−H(D) exchange and frequency considerations, we previously argued that the chromophore in P_r is C_5-Z,anti, C_{10}-E,anti, and C_{15}-Z,syn and that the chromophore in P_{fr} is C_5-Z,anti, C_{10}-E,-anti, and C_{15}-E,anti (*10*). The normal mode assignments in this work allow us to further test these assignments.

The vibrational spectra support the conclusion that the P_r and P_{fr} chromophores are fully protonated and cationic. The previous normal mode assignments of the 1570 cm^{-1} C═NH^+ stretching and ∼1320 cm^{-1} N−H rocking modes (*8−10*) are further corroborated here because these modes do not shift in the absence of N-deuteration. However, we do not know the location of the formal C═N bond(s) and of the cationic charge within the rings of the P_r and P_{fr} chromophores. In other phycobiliprotein systems such as C-phycocyanin (C-PC), the chromophore is cationic and stabilized by hydrogen bonding contact with an aspartate residue (*47*). This may explain the bathochromicity of the electronic absorption spectrum of C-PC (*48*). In our phytochrome calculations, the cationic charge resides in the C ring of the chromophore, and this model successfully predicts a number of vibrational spectroscopic differences between P_r and P_{fr}. The higher frequency ∼1320 cm^{-1} N−H rocking band in P_r supports the C_{15}═C_{16} Z chromophore geometry. The shift of this mode to lower frequency indicates a Z → E C_{15}═C_{16} configurational change consistent with the lower frequency 1301 cm^{-1} N−H band of the C_{15}═C_{16} E chromophore in P_{fr}.

The assignment of the C_{15}−HOOP in P_r provides information concerning the distortion about the C_{15}−methine bridge and therefore the planarity of the C and D rings (*49*). The 805 cm^{-1} HOOP mode is of moderate intensity in P_r. This is consistent with somewhat nonplanar C- and D-ring moieties. The 814 cm^{-1} HOOP mode is very intense in P_{fr}.

This means that the ring moiety in P_{fr} is highly distorted. These observations are consistent with the structures of P_r and P_{fr} depicted in Figure 6. P_r has moderately planar C and D rings because steric interactions are small, but P_{fr} has very nonplanar C and D rings due to the interaction of the C- and D-ring methyl groups.

Excited-State Structure and Reaction Dynamics. The chromophore structure in P_r is C_{15}-Z,syn, the chromophore structure in P_{fr} is C_{15}-E,anti, and the differences in the RR spectra of P_r and P_{fr} are consistent with geometrical changes about only the $C_{15}-$methine bridge (*9, 10*). This means that the photochemical isomerization mechanism must involve $C_{15}=C_{16}$ isomerization as originally suggested by work on phytochromopeptides (*50, 51*). The primary photochemistry could involve a simultaneous rotation of $C_{15}=C_{16}$ and $C_{14}-C_{15}$ bonds or a sequential $C_{15}=C_{16}$ isomerization followed by a thermal $C_{14}-C_{15}$ bond rotation (*9*). Our RR studies of chromophore structure in Lumi-R showed that the primary photochemistry involved just $C_{15}=C_{16}$ isomerization, and a four-state model was developed that used sequential $C_{15}-$methine bond rotations to describe the P_{fr} to P_r photochemistry (*10*). This model is quite similar to the C−T model developed to explain chromophore function in the photocycle of bacteriorhodopsin (*52*).

The mode assignments and relative RR intensities developed here provide even more information on the initial photochemical reaction dynamics. The intensity of RR modes in phytochrome reveals which modes are highly displaced in the excited state and hence are likely to play a role in the initial photochemical dynamics. The intense HOOP, torsional, and ring modes indicate that the initial nuclear displacements involve significant changes about several coordinates associated with the $C_{15}-$methine bridge.

The 805 cm^{-1} $C_{15}-$HOOP and 665 cm^{-1} torsional and ring modes of P_r are of moderate intensity, indicating moderate excited-state nuclear displacements. Thus, out-of-plane C−H and $C_{15}=C_{16}$ twisting displacements occur at the $C_{15}-$methine bridge in the excited state. These observations suggest that coupled in-plane ring rotations, torsions, and $C_{15}-$HOOP motions play a significant role in the initial photoisomerization dynamics.

In P_{fr}, the very intense HOOP mode at 814 cm^{-1} coupled with C−C and C=C torsional and in-plane ring rotation modes at ~670 cm^{-1} suggests very large specific excited-state nuclear displacements. The calculations further suggest that the intense HOOP modes are also mixed with in-plane ring rotations. The coupled ring rotation may indicate a photoisomerization trajectory that involves $C_{15}-$H displacement toward the opposite side of the methine bridge ($C_{15}-$H-flipping) and ring-sliding motion in the excited state; this may be an indication of simultaneous $C_{15}-$methine, C=C, and C−C bond rotations. Such large displacements are consistent with the very low fluorescence quantum yield and ultrafast isomerization because motion along the steeply sloping excited-state surface competes effectively with fluorescence emission.

The primary photoproducts of P_r and P_{fr} have been studied with Raman spectroscopy in an effort to reveal the photoisomerization mechanism (*10, 36*). The primary photoproduct of P_r, lumi-R, has a C_{15}-E,syn chromophore structure, indicating that only $C_{15}=C_{16}$ isomerization occurs upon P_r photoexcitation (*10*). Possibly, the reason simultaneous bond rotations is not observed in the primary photochemistry of P_r is because of a barrier which prevents D-ring motion; this barrier is presumably a result of protein contacts or the steric interaction of the chromophoric C- and D-ring methyl groups. The primary photoproduct of P_{fr}, lumi-F, has recently been studied by RR spectroscopy, and the chromophore structure is tentatively thought to be C_{15}-Z,syn (*25*). This suggests that the initial photochemistry involves a simultaneous concerted single and double bond isomerization. Simultaneous bond rotations have also been postulated in the photochemistry of the xanthopsin-containing photoactive yellow protein (*53*). Such models have also been proposed for bacteriorhodopsin *(54)* although their validity in that system has been convincingly challenged *(43)*.

The knowledge gained in studies of the role of nonbonded interactions in the photochemistry of rhodopsin may provide insight into the photochemical mechanism of phytochrome. In the 11-*cis*-retinal chromophore of rhodopsin, intramolecular nonbonded steric interaction between the 13-methyl group and the 10-hydrogen is responsible for the steep slope of the excited-state surface along the reactive $C_{11}=C_{12}$ torsional coordinate; this interaction is thought to contribute to the fast and efficient photochemistry (*26, 55)*. The calculated chromophore structures of P_r and P_{fr} phytochrome show that weak nonbonded steric interaction occurs between the C- and D-ring N−H groups in P_r but that strong nonbonded steric interaction occurs between the C- and D-ring methyl groups of P_{fr}. This suggests that the excited-state surface is relatively shallow for P_r but steeply sloped along the reaction coordinate for P_{fr}. We therefore expect that P_{fr} and rhodopsin will exhibit similar photochemical characteristics including strong coupling between the excited-state and ground-state photoproduct surfaces, rapid photoproduct formation, and weak spontaneous emission. In P_r, we expect weaker coupling between the ground- and excited-state surfaces and slower photochemistry.

For P_r, the weak coupling between ground- and excited-state surfaces is corroborated by the slow reaction time (τ = 24 ps), relatively strong fluorescence quantum yield ($\Phi = 5 \times 10^{-3}$), small fluorescence Stokes' shift (450 cm^{-1}) (*28, 56−58)*, and low reaction quantum yield (0.15) (*33, 59)*. These observations are consistent with the presence of a barrier to the photochemistry which has been identified by temperature dependence studies (*10*).

For P_{fr}, the strong coupling between the ground- and excited-state surfaces is corroborated by the very weak (less than 10^{-5}) fluorescence quantum yield. Based on the lack of fluorescence, the intense RR modes, and the expectant ultrafast photoisomerization, we would predict that the reaction quantum yield of P_{fr} would be very high. However, the reaction quantum yield of P_{fr} to P_r is only 0.069 (*33*). This may be due to thermal reactions back to P_{fr} after initial photoisomerization, strong chromophore−protein interaction that restricts the primary photochemistry at a point further along the reaction coordinate, or other intermolecular dissipative effects further along the reaction pathway. Recent experimental evidence supports the idea of rapid depopulation of the excited state of P_{fr} *(60)*.

SUPPORTING INFORMATION AVAILABLE

Supporting information on the details of the synthesis of d-PΦB and on the fitting of the SERDS spectra is available

(6 pages). This material is available free of charge via the Internet at http://pubs.acs.org.

REFERENCES

1. Kendrick, R. E., and Kronenberg, G. H. M. (1994) *Photomorphogenesis in Plants*, Martinus Nijhoff, Dordrecht.
2. Pratt, L. H. (1995) *Photochem. Photobiol. 61*, 10−21.
3. Vierstra, R. D., and Quail, P. H. (1986) in *Photomorphogenesis in Plants* (Kendrick, R. E., and Kronenberg, G. H. M., Eds.) pp 35−60, Martinus Nijhoff, Dordrecht.
4. Lagarias, J. C., and Rapoport, H. (1980) *J. Am. Chem. Soc. 102*, 4821−4828.
5. Bowler, C., Frohnmeyer, H., Schafer, E., Neuhaus, G., and Chua, N. (1997) *Acta Physiol. Plant. 19*, 475−483.
6. Elich, T., and Chory, J. (1997) *Cell 91*, 713−716.
7. Quail, P. (1997) *Bioessays 19*, 571−579.
8. Fodor, S. P. A., Lagarias, J. C., and Mathies, R. A. (1988) *Photochem. Photobiol. 48*, 129−136.
9. Fodor, S. P. A., Lagarias, J. C., and Mathies, R. A. (1990) *Biochemistry 29*, 11141−11146.
10. Andel, F., III, Lagarias, J. C., and Mathies, R. A. (1996) *Biochemistry 35*, 15997−16008.
11. Hildebrandt, P., Hoffmann, A., Lindemann, P., Heibel, G., Braslavsky, S. E., Schaffner, K., and Schrader, B. (1992) *Biochemistry 31*, 7957−7962.
12. Farrens, D. L., Holt, R. E., Rospendowski, B. N., Song, P.-S., and Cotton, T. M. (1989) *J. Am. Chem. Soc. 111*, 9162−9169.
13. Holt, R. E., Farrens, D. L., Song, P.-S., and Cotton, T. M. (1989) *J. Am. Chem. Soc. 111*, 9156−9162.
14. Mizutani, Y., Tokutomi, S., Aoyagi, K., Horitsu, K., and Kitagawa, T. (1991) *Biochemistry 30*, 10693−10700.
15. Mizutani, Y., Tokutomi, S., and Kitagawa, T. (1994) *Biochemistry 33*, 153−158.
16. Tokutomi, S., Mizutani, Y., Anni, H., and Kitagawa, T. (1990) *FEBS Lett. 269*, 341−344.
17. Kneip, C., Mozley, D., Hildebrandt, P., Gartner, W., Braslavsky, S. E., and Schaffner, K. (1997) *FEBS Lett. 414*, 23−26.
18. Knipp, B., Kneip, K., Matysik, J., Gartner, W., Hildebrandt, P., Braslavsky, S. E., and Schaffner, K. (1997) *Chem. Eur. J. 3*, 363−367.
19. Margulies, L., and Stockburger, M. (1979) *J. Am. Chem. Soc. 101*, 743−744.
20. Matysik, J., Hildebrandt, P., Smit, K., Mark, F., Gartner, W., Braslavsky, S. E., Schaffner, K., and Schrader, B. (1997) *J. Pharm. Biomed. Anal. 15*, 1319−1324.
21. Siebert, F., Grimm, R., Rudiger, W., Schmidt, G., and Scheer, H. (1990) *Eur. J. Biochem. 194*, 921−928.
22. Lin, S. W., Groesbeek, M., van der Hoef, I., Verdegem, P., Lugtenburg, J., and Mathies, R. A. (1998) *J. Phys. Chem. B 102*, 2787−2806.
23. Palings, I., van den Berg, E. M. M., Lugtenburg, J., and Mathies, R. A. (1989) *Biochemistry 28*, 1498−1507.
24. Li, L., Murphy, J. T., and Lagarias, J. C. (1995) *Biochemistry 34*, 7923−7930.
25. Andel, F., III (1998) Ph.D. Thesis, p 263, University of California, Berkeley.
26. Kochendoerfer, G. G., Verdegem, P. J. E., van der Hoef, I., Lugtenburg, J., and Mathies, R. A. (1996) *Biochemistry 35*, 16230−16240.
27. Murphy, J. T., and Lagarias, J. C. (1997) *Photochem. Photobiol. 65*, 750−758.
28. Andel, F., III, Hasson, K. C., Gai, F., Anfinrud, P. A., and Mathies, R. A. (1997) *Biospectroscopy 3*, 421−433.
29. Terry, M. J., Maines, M. D., and Lagarias, J. C. (1993) *J. Biol. Chem. 268*, 26099−26106.
30. Cornejo, J., Beale, S. I., Terry, M. J., and Lagarias, J. C. (1992) *J. Biol. Chem. 167*, 14790−14798.
31. Kim, M., Mathies, R. A., Hoff, W. D., and Hellingwerf, K. J. (1995) *Biochemistry 34*, 12669−12672.
32. Mathies, R. A., Oseroff, A. R., and Stryer, L. (1976) *Proc. Natl. Acad. Sci. U.S.A. 73*, 1−5.
33. Lagarias, J. L., Kelly, J. M., Cyr, K. L., and Smith, W. O. (1987) *Photochem. Photobiol. 46*, 5−13.
34. Shreve, A. P., Cherepy, N. J., and Mathies, R. A. (1992) *Appl. Spectrosc. 46*, 707−711.
35. Warshel, A., and Karplus, M. (1974) *J. Am. Chem. Soc. 96*, 5677−5689.
36. Matysik, J., Hildebrandt, P., Schlamann, W., Braslavsky, S., and Schaffner, K. (1995) *Biochemistry 34*, 10497−10507.
37. Myers, A. B., and Mathies, R. A. (1987) in *Resonance Raman Spectra of Polyenes and Aromatics* (Spiro, T. G., Ed.) pp 1−58, John Wiley & Sons, Inc., New York.
38. Abe, M., Kitagawa, T., and Kyogoku, Y. (1978) *J. Chem. Phys. 69*, 4526−4534.
39. Kitagawa, T., Kyogoku, Y., Iizuka, T., and Saito, M. I. (1976) *J. Am. Chem. Soc. 98*, 5169−5173.
40. Curry, B., Palings, I., Broek, A. D., Pardoen, J. A., Lugtenburg, J., and Mathies, R. (1985) in *Advances in Infrared and Raman Spectroscopy 12* (Clark, J. H., and Hester, R. E., Eds.) pp 115−178, Wiley, Heyden.
41. Li, L., and Lagarias, J. C. (1992) *J. Biol. Chem. 267*, 19204−19210.
42. Murphy, J. T., and Lagarias, J. C. (1997) *Curr. Biol. 7*, 870−876.
43. Mathies, R. A., and Li, X.-Y. (1995) *Biophys. Chem. 56*, 47−55.
44. Kitagawa, T. (1986) in *Spectroscopy of Biological Systems* (Clark, J. H., and Hester, R. E., Eds.) pp 443−481, John Wiley and Sons Ltd., New York.
45. Kitagawa, T., Iizuka, T., Ikeda-Saito, M., and Kyogoku, Y. (1975) *Chem. Lett.*, 849−852.
46. Spiro, T. G., and Strekas, T. C. (1974) *J. Am. Chem. Soc. 96*, 338−345.
47. Schirmer, T., Bode, W., and Huber, R. (1987) *J. Mol. Biol. 196*, 677−695.
48. Kikuchi, H., Sugimoto, T., and Mimuro, M. (1997) *Chem. Phys. Lett. 274*, 460−465.
49. Eyring, G., Curry, B., Broek, A., Lugtenburg, J., and Mathies, R. (1982) *Biochemistry 21*, 384−393.
50. Rudiger, W., Thummler, F., Cmiel, E., and Schneider, S. (1983) *Proc. Natl. Acad. Sci. U.S.A. 80*, 6244−6248.
51. Thummler, F., and Rudiger, W. (1983) *Tetrahedron 39*, 1943−1951.
52. Mathies, R. A., Lin, S. W., Ames, J. B., and Pollard, W. T. (1991) *Annu. Rev. Biophys. Biophys. Chem. 20*, 491−518.
53. Genick, U., Soltis, S., Kuhn, P., Canestrelli, I., and Getzoff, E. (1998) *Nature (London) 392*, 206−209.
54. Schulten, K., and Tavan, P. (1978) *Nature (London) 272*, 85−86.
55. Wang, Q., Kochendoerfer, G. G., Schoenlein, R. W., Verdegem, P. J. E., Lugtenburg, J., Mathies, R. A., and Shank, C. V. (1996) *J. Phys. Chem. 100*, 17388−17394.
56. Holzwarth, A. R., Wendler, J., Ruzsicska, B. P., Braslavsky, S. E., and Schaffner, K. (1984) *Biochim. Biophys. Acta 791*, 265−273.
57. Kandori, H., Yoshihara, K., and Tokutomi, S. (1992) *J. Am. Chem. Soc. 114*, 10958−10959.
58. Sineshchekov, V. A., Lapko, V. N., Sineshchekov, A. V., Kozhukh, G. V., and Udal'tsov, A. V. (1990) *J. Photochem. Photobiol. B: Biol. 5*, 219−229.
59. Gensch, T., Churio, M. S., Braslavsky, S. E., and Schaffner, K. (1996) *Photochem. Photobiol. 63*, 719−725.
60. Bischoff, M., Hermann, G., Rentsch, S., and Strehlow, D. (1998) *J. Phys. Chem.* 102, 4399−4404.

BI991688Z